Indian Journal of Engineering & Materials Sciences
Vol. 33, February 2026, pp. 36-50
DOI: 10.56042/ijems.v33i01.21617

Enhanced MPPT for PV systems using a two-stage hybrid fuzzy logic and P&O algorithm

Rajesh Kumar*, Ananyo Bhattacharya & Aanchal Singh S Vardhan
Department of Electrical Engineering, National Institute of Technology Jamshedpur 831 014, Jharkhand, India

Received: 15 July 2025; accepted: 09 January 2026

Photovoltaic (PV) systems have converted solar irradiance into electrical energy through PV cells that exhibit nonlinear voltage-current (V-I) characteristics. A key feature of these characteristics has been the maximum power point (MPP), where the product of voltage (V) and current (I) has reached its maximum, enabling optimal power extraction. The efficient operation of a PV system has required rapid and accurate Maximum Power Point Tracking (MPPT), especially in dynamically changing environmental conditions. This paper has presented a hybrid MPPT approach that has combined a Fuzzy Logic Controller (FLC) with the conventional Perturb and Observe (P&O) algorithm. The proposed two-stage control scheme has continuously identified and adjusted the MPP in response to variations in irradiance and temperature, including partial shading (PS) scenarios. In the first stage, the FLC has provided an intelligent initial estimate of the MPP region to improve the convergence speed of the P&O algorithm. In the second stage, another FLC has dynamically adjusted the step size of the P&O algorithm to improve response and reduce oscillations. The hybrid FLC-P&O algorithm has been validated through simulations under various conditions, including steady irradiance, sudden changes in sunlight, and partial shading of varying severity. The results have demonstrated that the proposed controller has achieved high tracking efficiency and has effectively overcome the limitations of the conventional P&O algorithm, particularly under non-uniform and rapidly changing environmental conditions.

Keywords: Fuzzy logic controller, Perturb and observe, Hybrid MPPT, PV system, Boost converter, Partial shading

1 Introduction

Solar energy is widely recognized as one of the most promising renewable energy sources because it is abundant, sustainable, and environmentally friendly. Over the past decades, much research has been conducted on both increasing the efficiency of photovoltaic (PV) systems and developing novel applications of clean energy technologies[1]. However, PV systems, having relatively recently come into existence in the energy landscape, convert directly to electrical energy from solar irradiance as a potential alternative to the traditional methods of fossil fuel-based power generation[2]. The systems described here can be used to provide power to an extensive number of applications, from hydrogen generation units to grid-connected networks to standalone systems, including pumps for water[3]. However, environmental factors such as irradiance (G), temperature, and partial shading (PS) significantly affect the output power of PV systems[4]. Maximum power point tracking (MPPT) algorithms are essential for extracting the highest possible energy from a PV system, since the maximum power point (MPP) shifts continuously with changing environmental conditions[5]. In general, MPPT algorithms are paired with power electronic converters to continuously adjust the operating point of PV systems, ensuring maximum power transfer under changing conditions[6]. The most practical and cost-effective can be from different enhancement strategies, which can be improving MPPT algorithms rather than PV module materials or converter, as in general, technological and economic limitations can constrain such technology direction changes[7]. Therefore, MPPT methodologies have been developed considerably so far, and one of them, the direct method, is the most attempted one, and the widely implemented one is the Perturb & Observe (P&O) algorithm[8]. These algorithms are crucial in enabling continuous real-time MPPT of PV systems by modifying operating parameters to follow the MPP.

Even though it's commonly used, the MPP found using a standard MPPT method like the P&O algorithm has significant problems, including constant fluctuations at the MPP, a slow response to changes, being easily affected by local peaks during PS, and

*Corresponding author (E-mail: rajeshdce10@gmail.com)

low accuracy during quick changes in environmental conditions[9]. However, the outcome of these flaws could be energy losses and decreased system performance. In response, endless quantities of research have been spent to perfect these algorithms or to formulate hybrid approaches mixing traditional methods with advanced control strategies. Although the P&O technique is widely used for its simplicity and low implementation cost, its fixed step size introduces inherent limitations near the MPP, leading to noticeable oscillatory behaviour[10]. Pushing a smaller step size towards convergence leads to steady-state accuracy with a simultaneous decrease in convergence speed, while a larger step size increases steady-state tracking speed at the cost of steady-state accuracy[11]. In order to overcome these trade-offs, many modifications of the P&O algorithm have been suggested. Consequently, one effective method is to combine fuzzy logic controllers (FLCs) that are well suited to problems with nonlinearity and uncertainty[12]. The adaptability of FLCs, which can be seamlessly joined with conventional MPPT methods, makes them attractive for cross-boundary applications between converters. Thorough tests, both in the laboratory and in complex control environments like industrial automation, robots, and solar cells, have proven their strong performance. The MPPT performance is improved using a hybrid FLC-P&O algorithm based on variable step size (VSS)[13]. In contrast to most of the methods previously used, this method dynamically adjusts the step size in response to the system conditions, thus eliminating oscillations and improving both transient and steady-state performance[14]. In other words, studies show that this method can lead to up to a 0.38% increase in the tracking efficiency over the P&O methods[15]. In addition, this paper develops an efficient two-stage MPPT strategy to help further limit the limitations of conventional techniques. In this method, the FLC estimates the MPP but gives a rough estimate so that convergence would be accelerated, and refined tracking is applied by the P&O algorithm. This hybrid approach offers an effective compromise between rapid tracking and high accuracy, supporting real-time performance even under changing environmental conditions.

This paper aims to develop and evaluate a novel hybrid MPPT strategy that integrates an FLC and P&O algorithm in a two-stage architecture to achieve rapid tracking, reduced steady-state oscillations, and high efficiency under dynamically changing and non-uniform irradiance conditions, outperforming the traditional P&O algorithm.

This study is unique because it created a two-stage hybrid MPPT algorithm that integrates a modified FLC with the conventional P&O algorithm. In the first stage, a variant of the FLC generates an intelligent initial estimate of the MPP, which significantly accelerates the convergence of the P&O algorithm. In the second stage, secondary FLC dynamically adjusts the VSS of the P&O algorithm in real time to minimize steady state oscillations and enhance responsiveness under rapid environmental changes. This adaptive combination of intelligent estimation and perturbation-based refinement enables superior tracking performance in dynamic conditions.

The proposed hybrid FLC-P&O control strategy is implemented and simulated in MATLAB/Simulink under various operating scenarios, including uniform irradiance, sudden irradiance transitions, and partial shading conditions (PSC) of different severities. A comparative analysis with the conventional P&O and standalone VSS-P&O techniques confirms that the proposed method offers enhanced tracking efficiency, quicker convergence to the MPP, and greater overall system stability. These improvements make the approach both practically viable and economically efficient for real-time PV system optimization.

2 Materials and Methods

2.1 Model of PV cell

Semiconductor-based cells are employed in PV systems to convert solar energy into electricity. These cells are then combined into sealed modules that can be connected in parallel, series, or combination to form a PV array [16]. Performance of PV cells is affected by environmental factors such as temperature and G; voltage (V) and current (I) output are affected. When sunlight photons excite electrons in the semiconductor, electricity is produced; this reaction is known as the PV effect[17]. Figure 1 shows a system model that uses equations to simulate and optimize PV module behavior, enhancing energy output predictions and system efficiency.

Using the following formula, the module's saturation current ($\tilde{I}_{SC}$) depends strongly on the cell temperature. This equation allows us to model in terms of temperature the influence it has on the saturation current and hence on the entire performance of the PV module.

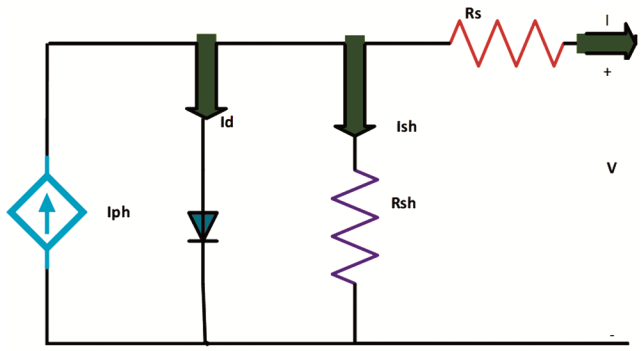

Fig. 1 — PV cell's equivalent circuit.

$$I_{ph} = [I_{sc} + K_i(T - 298)] \times \frac{I_r}{1000} \quad \ldots(1)$$

$$I_{rs} = I_{sc}/[\exp(qV_{oc}/N_s knT)) - 1] \quad \ldots(2)$$

$$I_0 = I_{rs}\left[\frac{T}{T_r}\right]^3 \exp\left[\frac{q \times E_{g0}}{nk}\left(\frac{1}{T} - \frac{1}{T_r}\right)\right] \quad \ldots(3)$$

Other factors being held constant, the output power from the system is inversely proportional to temperature and directly proportional to irradiance. The MPP is tracked by a topology and converter in the presence of temperature and irradiance variation. Because PV systems have nonlinear characteristics, these factors have a major impact on their performance and efficiency.

$$I_0 = I_{rs}\left[\frac{T}{T_r}\right]^3 \exp\left[\frac{q \times E_{g0}}{nk}\left(\frac{T_r - T}{T_r T}\right)\right] \quad \ldots(4)$$

$$V_t = \frac{k \times T}{q} \text{ and } I_{sh} = \frac{V \times (N_p + I\,N_s)\,R_s}{R_{sh} N_s} \quad \ldots(5)$$

2.2 DC to DC boost converter

In this study, a boost converter is used to control the energy transfer from the PV modules to the load resistance (RL) in the MPPT system. The DC to DC converter adjusts the power transfer by modifying the duty cycle (α), which can vary depending on the characteristics of the electronic components, allowing the voltage to shift from one level to another desired output voltage (Vout)[18]. To ensure the best efficiency value under the requirement, the condition of the DC–DC converter is of great importance. For low- to moderate-electric-power applications, MOSFETs and standard diodes are selected as the elements of interest, as they are typically used. After the inductor's size and the switching losses have been balanced, the switching device's frequency is set to 25 kHz. It covers the optimal boost converter topology for various MPPT techniques and the process of MPP. It also discusses the use of a converter in PV systems to

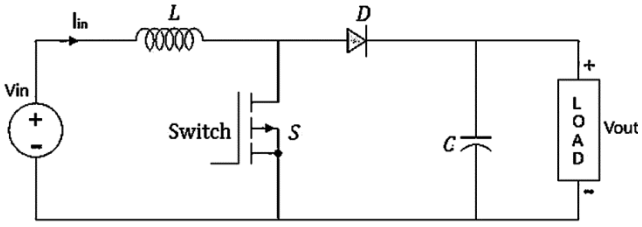

Fig. 2 — Circuit diagram of a boost converter.

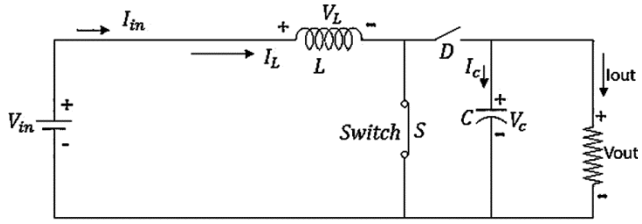

Fig. 3 — When circuit S is ON.

maintain the output of the PV source. The V-I converter transforms the DC input voltage into the DC Vout with low converter loss[19]. The converter's control signal δ(t) stays low for T_{OFF} and high for T_{ON}. The generated energy varies based on atmospheric conditions, and turning the switch on reduces voltage and watt loss. Switching off decreases power and current. α is determined to control the average output (Vout) and maintain a constant switching time [20]. Figure 2 shows a circuit of a boost converter voltage from input to output, ensuring the inductor's current never reaches 0.

$$\alpha = {}^{T_{on}}/_{T} \quad \ldots(6)$$

2.2.1 Case 1: When S is on & D is off : Figure 3 shows the switch (S) in open states with the diode as a barrier to prevent a reverse current flow. The switch allows current to pass in the closed state and in the open state, the diode blocks reverse current to guarantee correct current direction and circuit stability.

Inductor polarity is based on the direction of current flow. When the switch is fully on, reverse biasing "turns off" the current, resulting in a Vout and a voltage spike. The total time represents the combination of the on and off durations of the switch within one complete operating cycle.

$$V_L = L.\frac{dI_L}{dt} = V_{in} \quad \ldots(7)$$

$$\frac{dI_L}{dt} = \frac{V_{in}}{L} \; also \; \frac{dI_L}{dt} = \frac{\Delta I_L}{\Delta t} = \frac{\Delta I_L}{\alpha T} = \frac{V_{in}}{L} \quad \ldots(8)$$

Since the switch remains closed for a duration $T_{ON} = \alpha\ T$, thus $\Delta t = \alpha\ T$, then, the inductor current increases linearly according to

$$\Delta I_L = (V_{in}/L)\alpha T \quad \ldots(9)$$

2.2.2 Case 2: When S is off & the D is on: Figure 4 shows the operation of the S when closed. When the switch is open, it prevents current circulation, and diode passes the current, which is necessary for current direction and proper circuit operation.

$$V_{in} - V_L - V_{out} = 0, V_L = V_{in} - V_{out} \quad \ldots(10)$$

$$V_L = L\frac{dI_L}{dt} = V_{in} - V_{out} \quad \ldots(11)$$

$$\frac{dI_L}{dt} = \frac{V_{in}-V_{out}}{L} \quad \ldots(12)$$

$$Now, \frac{dI_L}{dt} = \frac{\Delta I_L}{\Delta t} = \frac{\Delta I_L}{(1-\alpha)T} = \frac{V_{in}-V_{out}}{L} \quad \ldots(13)$$

$$\Delta I_L = (1-\alpha)(\frac{V_{in}-V_{out}}{L})T \quad \ldots(14)$$

From the equation, it states that the sum of the I change rates is 0 since there is no current change in mode 2 when the S is open, thus it implies the current is constant during this time period.

$$\Delta i_L(mode\ 1) + \Delta i_L(mode\ 2) = 0 \quad \ldots(15)$$

$$\left(\frac{V_{in}}{L}\right)\alpha T + (\frac{V_{in}-V_{out}}{L})(1-\alpha) \quad \ldots(16)$$

Simplifying, we get:

$$\frac{V_{out}}{V_{in}} = \frac{1}{1-\alpha} \quad \ldots(17)$$

The PV array output acts as the input voltage (V_{IN}) to the boost converter, with its duty cycle (α) adjusted according to the MPPT algorithm. The boost converter depends on the action of the MOSFET; for example, by switching the current from the charge to the discharge cycle of the inductor. Continuous conduction mode implies that the α, defined as the ratio of on-time to total time and determining the relationship between V_{IN} and V_{OUT} voltage, is controlled using a PWM signal and constrained within $0 \leq \alpha \leq 1$. The RL should be equal to or higher than the internal resistance at MPP of the PV array (RMPP) to get best MPP tracking. The RMPP was determined by simulating under different irradiance levels (200–1000 W/m²). The MPP decreased as light reduced from 1000 W/m² to 200 W/m², from 249 W to 49.15 W, while RMPP increased from 3.61 Ω to 17.75 Ω. RL ≥ RMPP was guaranteed under all conditions by choosing the RL = 53 Ω.

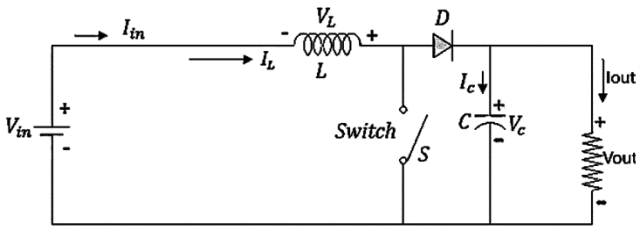

Fig. 4 — When S is OFF.

In this study, the allowed variation in input current (Δi_{pv}) at the MPP during the peak sunlight level (1000 W/m²) is used to choose the inductor value for the boost converter. From Equation (11), we can see that a larger inductance will lead to less current variation. That a higher inductance will lead to a lower current ripple. A switching frequency (fs) of 25 KHz, to reduce oscillation around the MPP, and L = 1.1 m, to preserve a 1% input current ripple. Furthermore, input and output capacitor values are calculated so that the output voltage ripples (ΔVo) are below 2% to have stable voltage regulation at the converter output. Figures 5(a) and 5(b) illustrate the I–V and P–V characteristics of the PV system, demonstrating that factors such as irradiance, temperature, and humidity significantly influence the systems output power and overall efficiency.

2.3 MPPT controllers

MPPT is an important characteristic of PV solar systems. It is an approach to control strategy based upon a set of programmed algorithms embedded in charge controllers that continuously extract the highest possible output P from a PV array[21]. MPPT algorithms are also needed since drastic variations in environmental conditions, such as G, shading levels, temperature, or module electrical characteristics, need the ability to adapt to them as they change quickly (e.g., solar irradiance). In other words, the aim of the MPPT technique is to always reach and track the optimum point of PV (MPP in a module: the point on the I-V curve for which the product of V and I is maximized). Due to the change of irradiance and temperature from day to day, MPP shifts dynamically[22]. As a result, it is critical that the MPPT algorithm continuously react to these variations in order to continuously harvest optimal amounts of energy. Usually, an MPPT controller is realized via a DC-to-DC converter in series with the PV array or in series with the energy storage system (or the inverter). The power transfer to the load is maximized via this converter through adjustment of the modules operating V and I to the MPP under the environmental conditions[23]. In the literature, a lot of MPPT

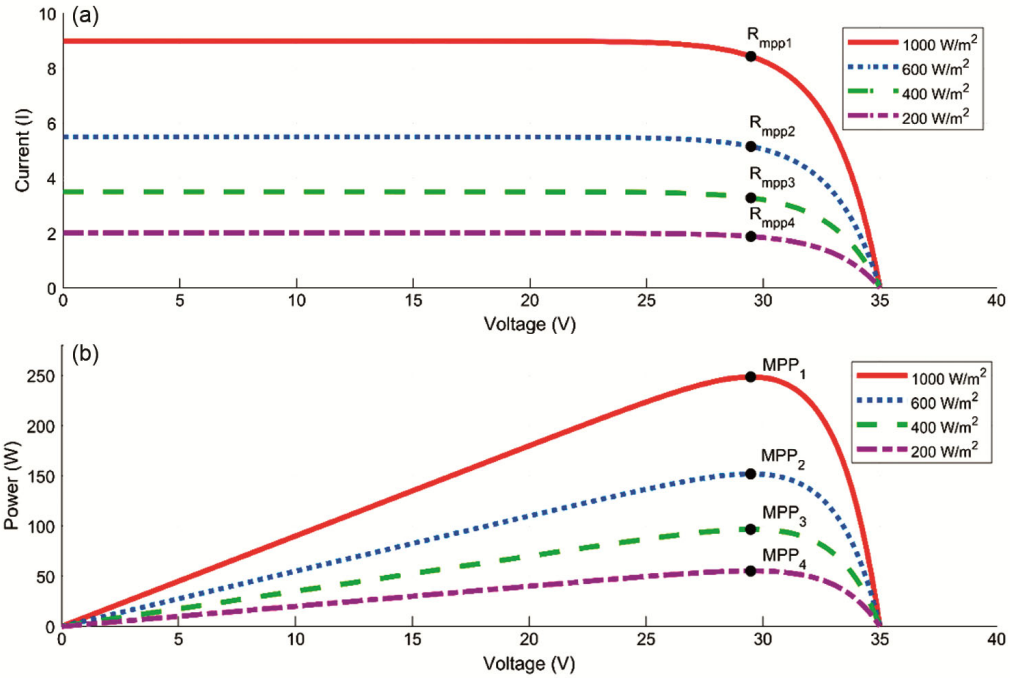

Fig. 5 — PV Module for different levels of insolation (a) I-V curve and (b) P-V curve.

algorithms have been developed, analyzed, or optimized to improve performance under different scenarios of operation. The objective of these techniques is to adapt to changes in irradiance as well as temperature and to optimize energy yield. At the peak power V-I, the PV module has a specific output V-I that characterizes the MPP. For example, a standard PV module running at a cell temperature of 25°C provides about 17 V maximum Vout. Yet, temperature varies the voltage: under high temperature it decreases to about 15 V, and at low variations of these stresses highlight the need of having high performance and adaptable MPPT algorithms to efficiently operate across various environmental conditions in PV systems.

2.4 P&O method

The P&O technique controls the PV system by changing the operating voltage and monitoring the relationship between voltage and power output[24]. This method causes oscillation, especially in unstable conditions, and can slow down the MPPT's response to weather changes. Current is controlled by the controller in proportion to power changes, increasing when power increases and decreasing when it decreases. PV voltage and current are measured using the technique, as there is a MATLAB embedded function, operating at a kHz frequency[25]. The current adjustment is decided by the controller comparing P(k) and P(k-1). Figure 6 displays the P&O flowchart. The technique introduces voltage perturbations in each MPPT cycle, which fluctuates the output power about the MPP and potentially causes output power loss. A dynamic constant that is a function of time is used to adjust the duty ratio such that the duty ratio matches prior power variations.

2.5 FLC

The FLC was developed by Lotfi A. Zadeh in 1965, and it is a viable way to control system nonlinearity, imprecise system inputs, and the need for an exact mathematical model. The four main components of FLC are fuzzification, base rule, engine inference, and defuzzification. This study proposes a two-stage hybrid MPPT algorithm that integrates FLC with the traditional P&O method[26]. FLC also speeds up the convergence speed of P&O in the 1st stage to provide an initial estimate near the MPP. In the 2nd stage, another FLC also dynamically tunes the P&O-VSS to achieve steady-state stability and fast transient response. Fast tracking but high-power oscillations near MPP are used with conventional P&O, in which a large fixed VSS is utilized, while small VSSs are used for low-power oscillations and slow response to irradiance changes[27]. The limitations of the use of conventional MPPT with

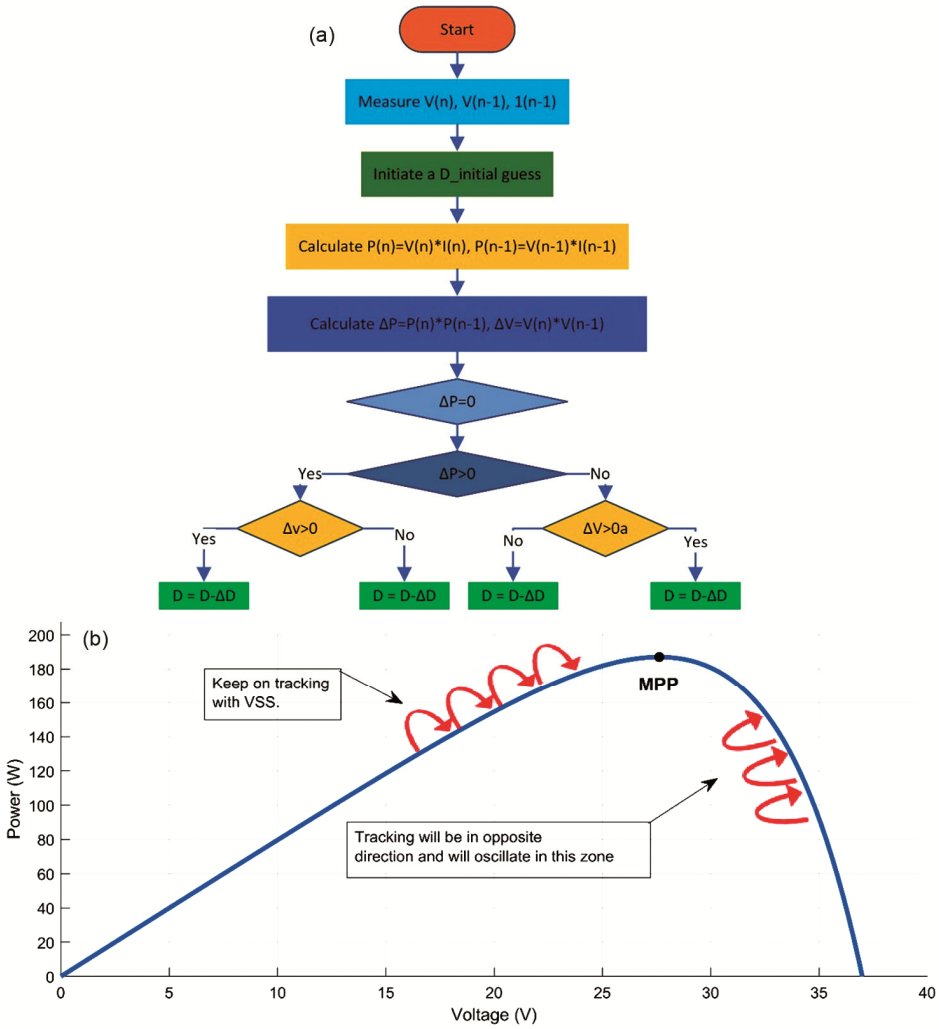

Fig. 6 — Functioning of P&O MPPT (a) Flow diagram of P&O method and (b) P&O MPPT based tracking under constant irradiation.

a fixed VSS are overcome by the variable VSS approach proposed, which is tuned using FLC and gives better performance under dynamic conditions[28]. A first FLC with two inputs based on Voc and Isc and one output as the initial estimate (Din) is used. A modeled model is illustrated in Fig. 7 and Table 1 with five steps, namely very small (VS), small (S), medium (M), large (L), and very large (VL), characterizing each input and output variable.

In this stage, the second FLC determines the appropriate VSS (Δ) for the P&O algorithm. It has two inputs: Error (E), representing the slope of the PV curves indicating MPP proximity, and change in Error (ΔE), which assesses the direction of movement toward MPP. The output, ΔD, is provided to the DC-to-DC converter to regulate the load power accordingly. Each input consists of five fuzzy sets: NL, NS, ZE, PS, and PL, while the output consists of VS, S, M, L, and VL, as defined in Table 2. A total of 25 fuzzy rules are applied using the MIN-MAX implication method. Figure 8 displays the input and output membership functions.

Figure 9 illustrates the flowchart of the proposed controller, which employs a dual-stage MPPT scheme combining FLC and the P&O algorithm. In the first stage, the FLC predicts an initial α based on real-time V and I measurements. The power and voltage changes are calculated to drive the P&O algorithm into fine-tuning the D for accurate tracking to MPP. The second FLC dynamically adjusts the P&O VSS to minimize steady-state oscillations and improve transient response[29]. The membership function ranges of Figures 6 and 8 were defined by using expert knowledge and experimental data in order to guarantee a correct input-output representation in typical PV operating conditions.

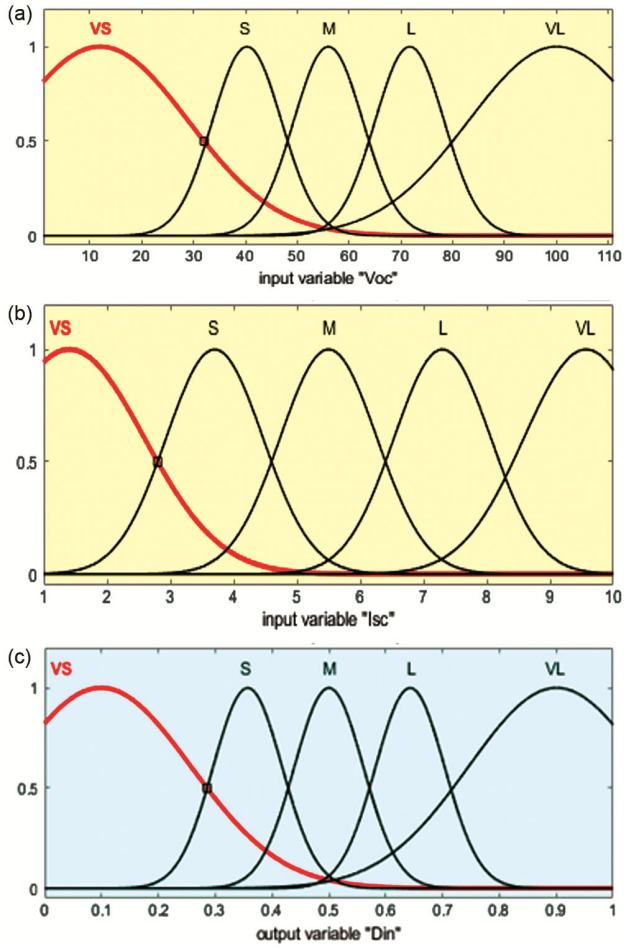

Fig. 7 — Membership functions of first-stage FLC for (a) Voc, (b) Isc, and (c) Initial duty cycle (Di).

Table 1 — Fuzzy inference.

Voc/Isc	VS	S	M	L	VL
VS	M	M	S	L	VL
S	M	M	M	L	VL
M	VS	S	M	L	VL
L	VS	S	M	L	M
VL	VS	S	L	M	M

Table 2 — Inference of FLC

E/E	NL	NS	ZE	PS	PL
NL	VL	NL	S	S	VS
NS	VS	VS	S	VL	S
ZE	VS	VS	S	VL	S
PS	S	S	VL	VL	VL
PL	S	S	VL	VL	VL

3 Results and Discussion

3.1 Model connection of system

The power output of the PV module is calculated by its power curves, which relate V and I to incident irradiance and ambient temperatures. The calculation

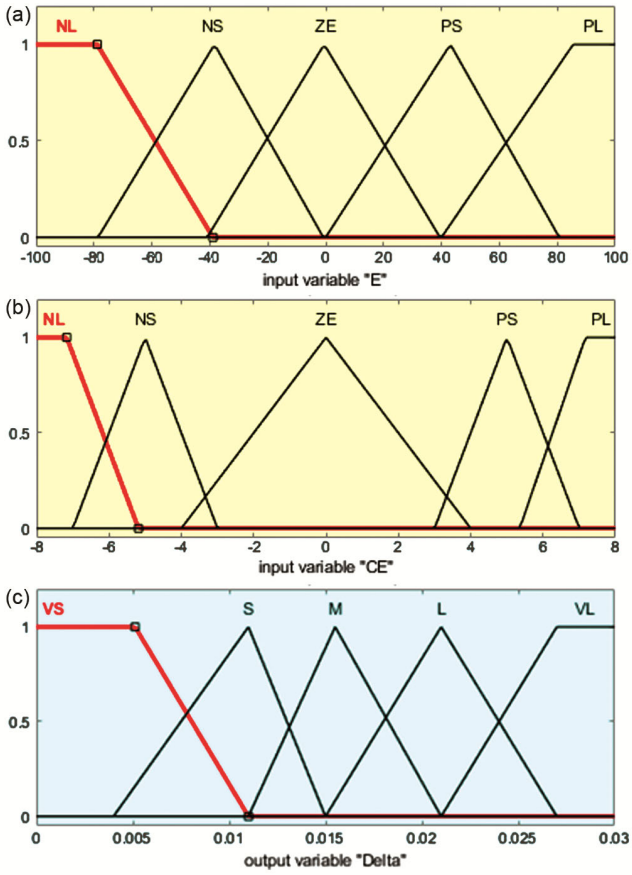

Fig. 8 — Membership functions of second-stage FLC for (a) Error (E), (b) Change in error (ΔE), and (c) Duty cycle adjustment (ΔD).

procedure follows the steps illustrated in Figures 10 to 17.

3.2 Results of the proposed system

MATLAB/Simulink simulations on the suggested FLC-P&O-FLC hybrid VSS-MPPT controller's performance are carried out under varying weather conditions. The system comprises a PV module and the proposed algorithm-controlled boost converter to obtain the optimal duty adjustment and to achieve the global maximum power point (GMPP) across different irradiance levels (as given in Table 3). This is used to assess the controller's tracking efficiency over these scenarios, and the PV model parameters are detailed in Table 4.

Figures 18, 19, and 20 show how the proposed system is analyzed under various PSC, i.e., weak, moderate, and strong sudden changes in irradiance and uniform irradiations. In its performance, the proposed control performed more effectively than the traditional P&O in uniform irradiance, sudden changes in irradiance, and PS. The P&Os sped up the

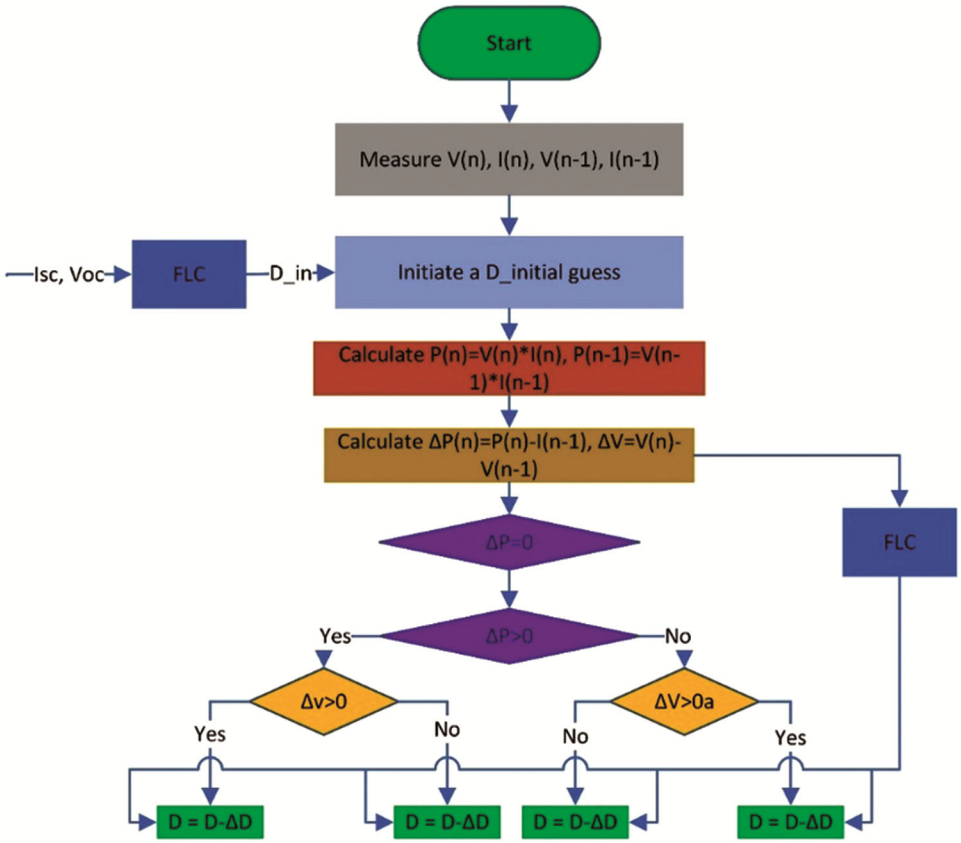

Fig. 9 — FLC-P&O-based VSS.

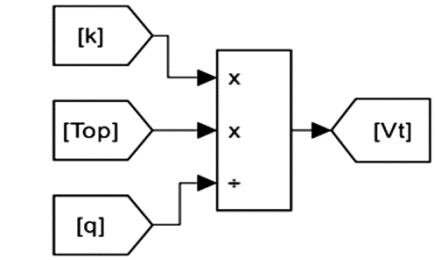

Fig. 10 — Thermal voltage equation modelling.

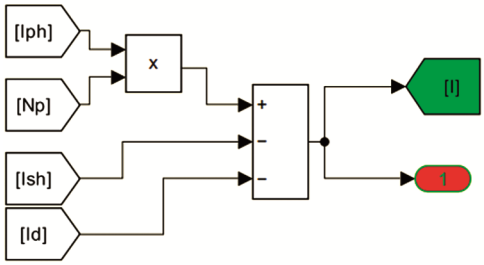

Fig. 11 — Load current equation modelling.

convergence and improved the tracking accuracy and GMPP identification compared to the conventional P&Os, which were sometimes stuck at the local maximum power point (LMPP).

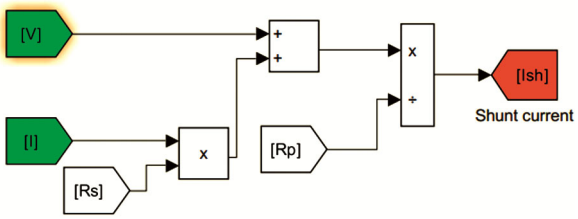

Fig. 12 — Shunt current equation modelling.

3.2.1 Uniform irradiation

Figure 21 evaluates the conventional P&O against the suggested controller under conditions of consistent solar exposure, where each PV panel is subjected to 1000 W/m². The results indicate that the new controller more rapidly achieves the MPPT, taking only = 0.14s.

3.2.2 Sudden irradiation change

To assess the system's performance under rapidly changing irradiance, the solar irradiance was abruptly decreased from 1000 w/m² to 500 w/m² and subsequently back to 1000 w/m². In comparison to the conventional P&O, Figures 22 & 23 illustrate an enhanced dynamic irradiance variation response and a higher tracking efficiency.

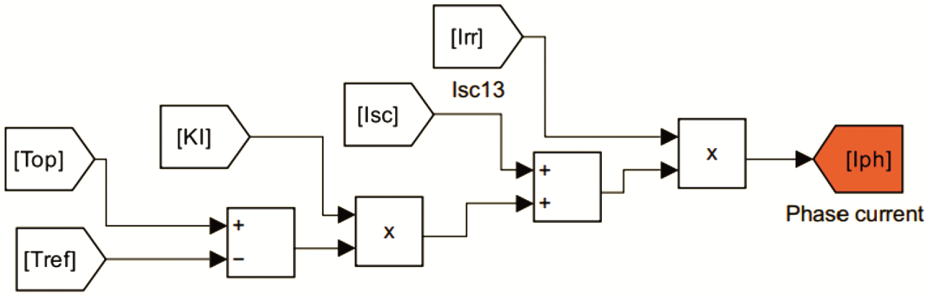

Fig. 13 — Phase current equation modelling.

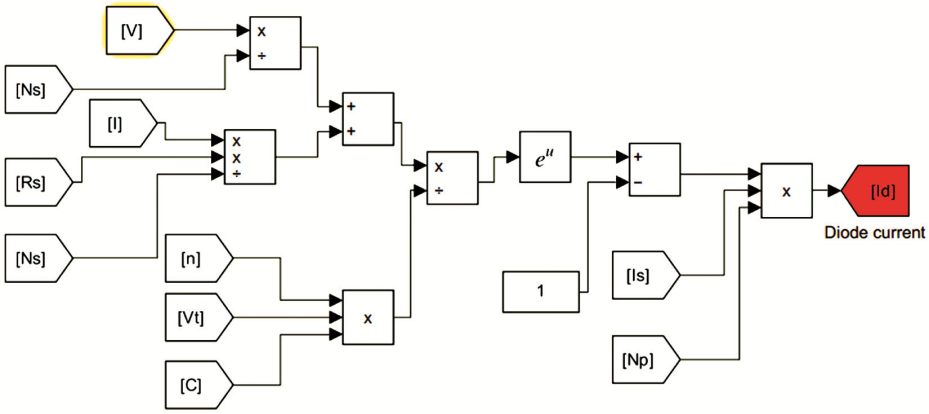

Fig. 14 — Diode current equation modelling.

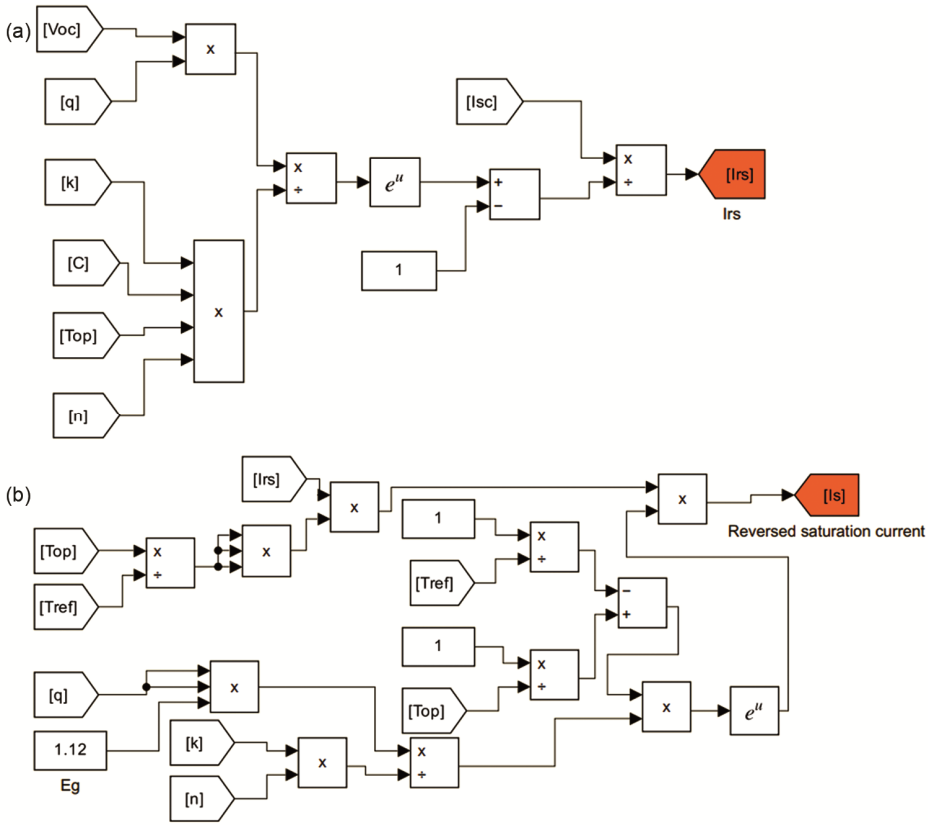

Fig. 15 — Reverse saturation current modelling (a) Saturation current reverse model at top and (b) Saturation current reverse.

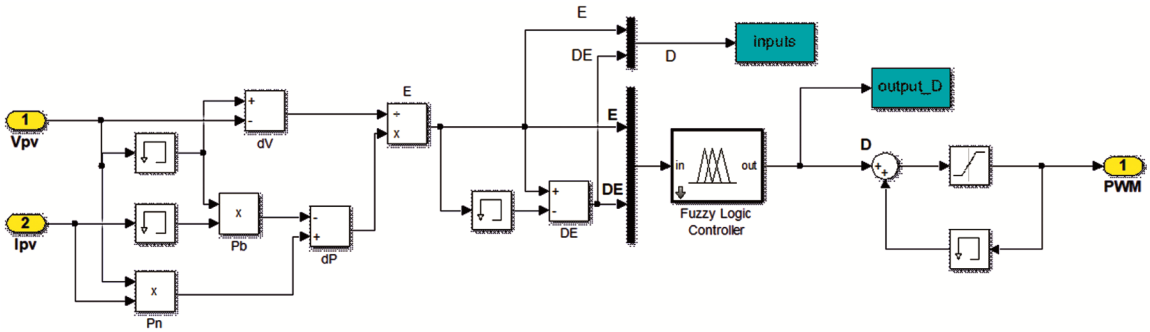

Fig. 16 — FLC based MPPT block connection.

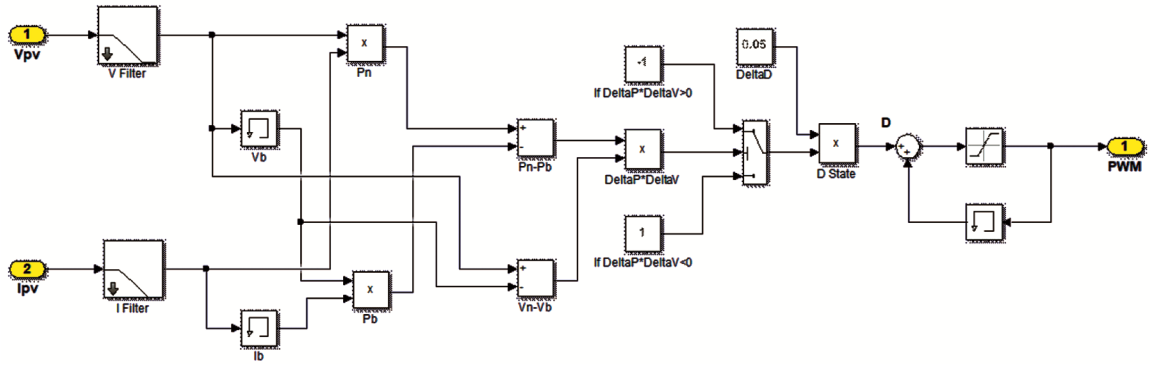

Fig. 17 — P&O based MPPT block connection.

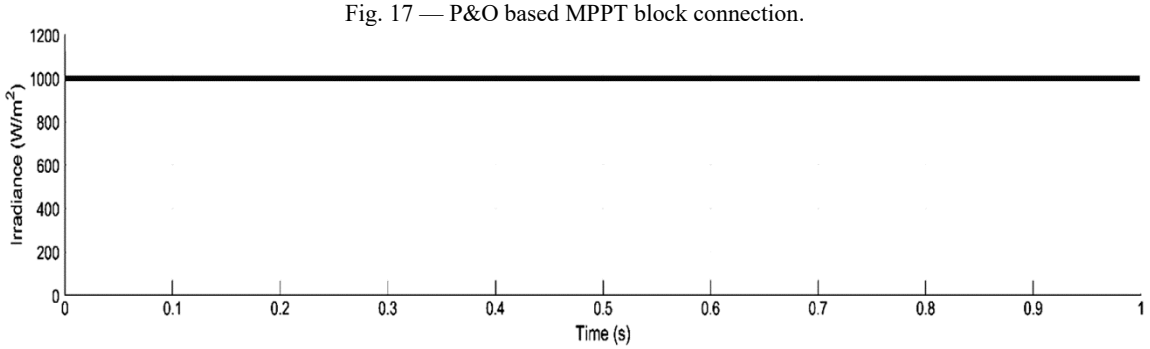

Fig. 18 — For MPPT performance testing, a uniform irradiation pattern.

Table 3 — Specification of the boost converter.

Switching Frequency	10kHz
Input Capacitor (Cin)	100 µF
Output Capacitor (Cout)	200µF
Inductor (L)	13mH
Resistive Load (R)	30 Ω

Table 4— Specification of the PV module.

MPP	250.2W
Voltage in open circuit (V_{OC})	37.3V
Voltage at MPP (V_{MPP})	30.7V
Short Circuit Current (I_{SC})	8.66A
Current at MPP (I_{MPP})	8.15A
Temp. Coefficient of V_{OC}	-0.36901
Temp. Coefficient of I_{SC}	0.086998
Number in Cells of series (Ns)	60
Temp. of the operating Cells	25°C

3.2.3 Partial irradiation shading

To validate that method effectively, several PSC scenarios have been simulated, each being weak, moderate, or strong. An example of how the FLC-P&O-FLC would perform under these conditions is given by the results. The proposed approach is also compared to the conventional P&O methods, highlighting its superior tracking capability and robustness in accurately locating and stabilizing at the GMPP in complex shading conditions. For the first two PV panels, they received uniform irradiance of 1000 W/m², and the third received irradiance of 750 W/m², as depicted in Table 5. The P–V characteristics of the PV array in PS are shown in Figure 24, in which the two GMPPs and an LMPP are indicated by

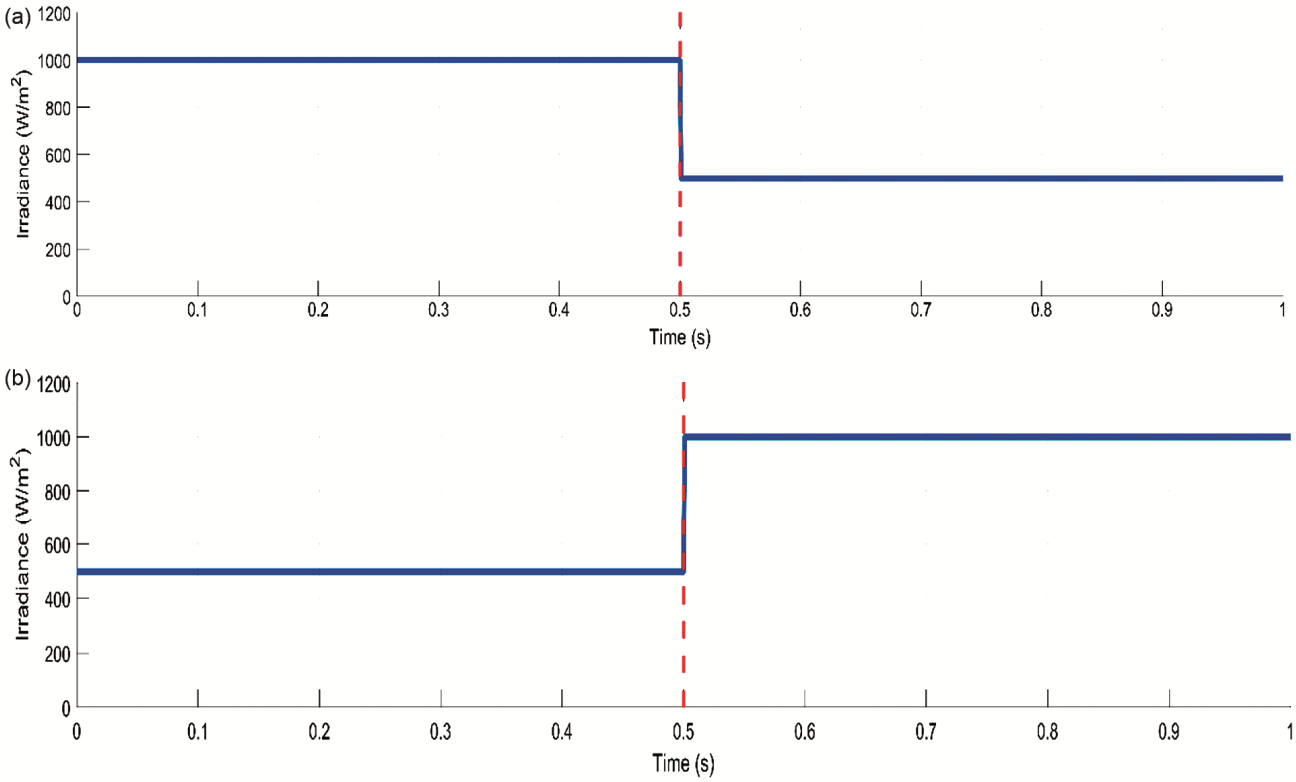

Fig. 19 — The MPPT performance test uses a sudden change in the irradiation pattern (a) Radiation levels suddenly dropped from 1000 w/m^2 to 500 w/m^2 and (b) Radiation levels quickly increased from 500 w/m^2 to 1000 w/m^2.

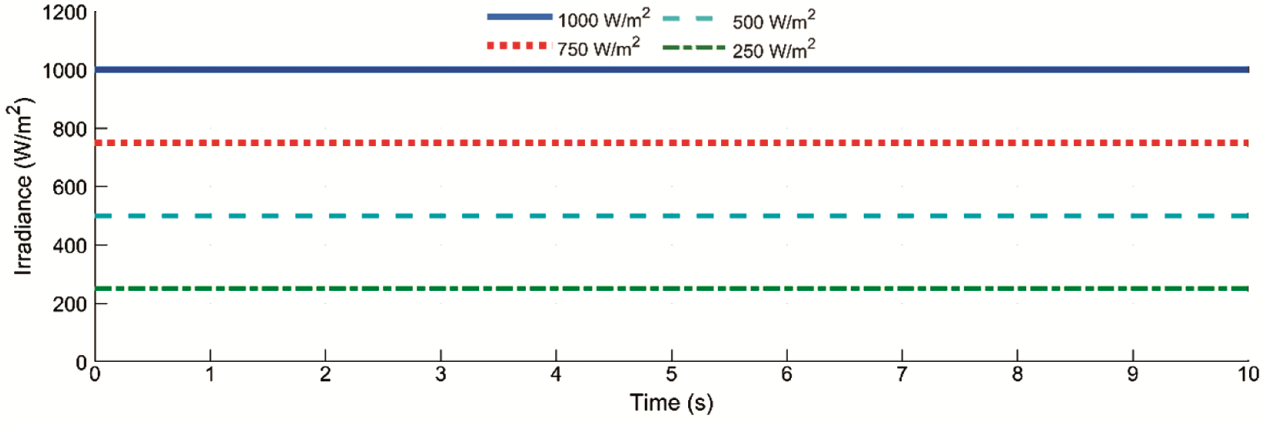

Fig. 20 — For the MPPT performance testing, PS patterns (strong 250 w/m², moderate 500 w/m², and weak 750 w/m²) were utilized.

two distinct peaks. During the simulation period, the proposed controller is capable of distinguishing between GMPP and LMPP. It is shown in Figures 25–27 to track the GMPP in a fast, dynamic way under shading conditions. On the other hand, unlike the conventional P&O methods, the LMPP is not reached by the traditional P&O technique and gets trapped instead. The P&O component follows the fuzzy controller component to effectively estimate an initial D close to the GMPP and refine it to achieve the best power extraction from the PV system.

Table 6 provides a performance comparison between the proposed hybrid controller and the traditional P&O algorithms in different operating conditions. The results demonstrate that the proposed controller consistently achieves higher tracking efficiency, faster response, and superior GMPP tracking accuracy across all irradiance levels, including rapidly changing irradiance and PSC.

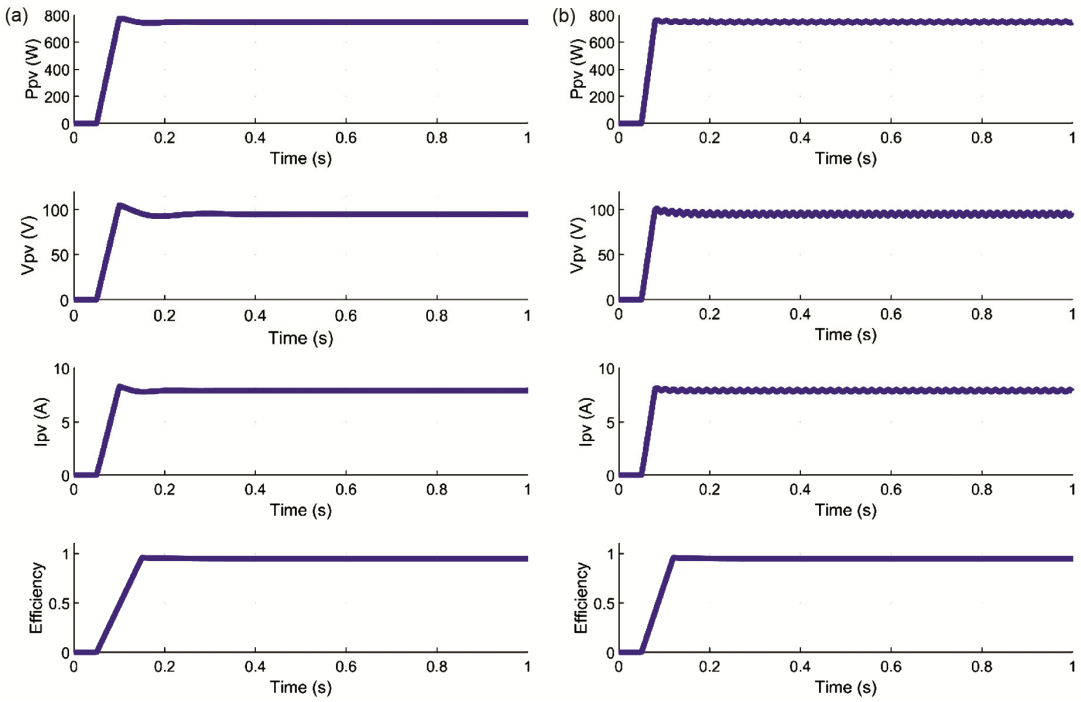

Fig. 21 — PV system with consistent irradiation (1000 W/m^2) (a) Conventional P&O and (b) Proposed FLC-P&O-FLC controller.

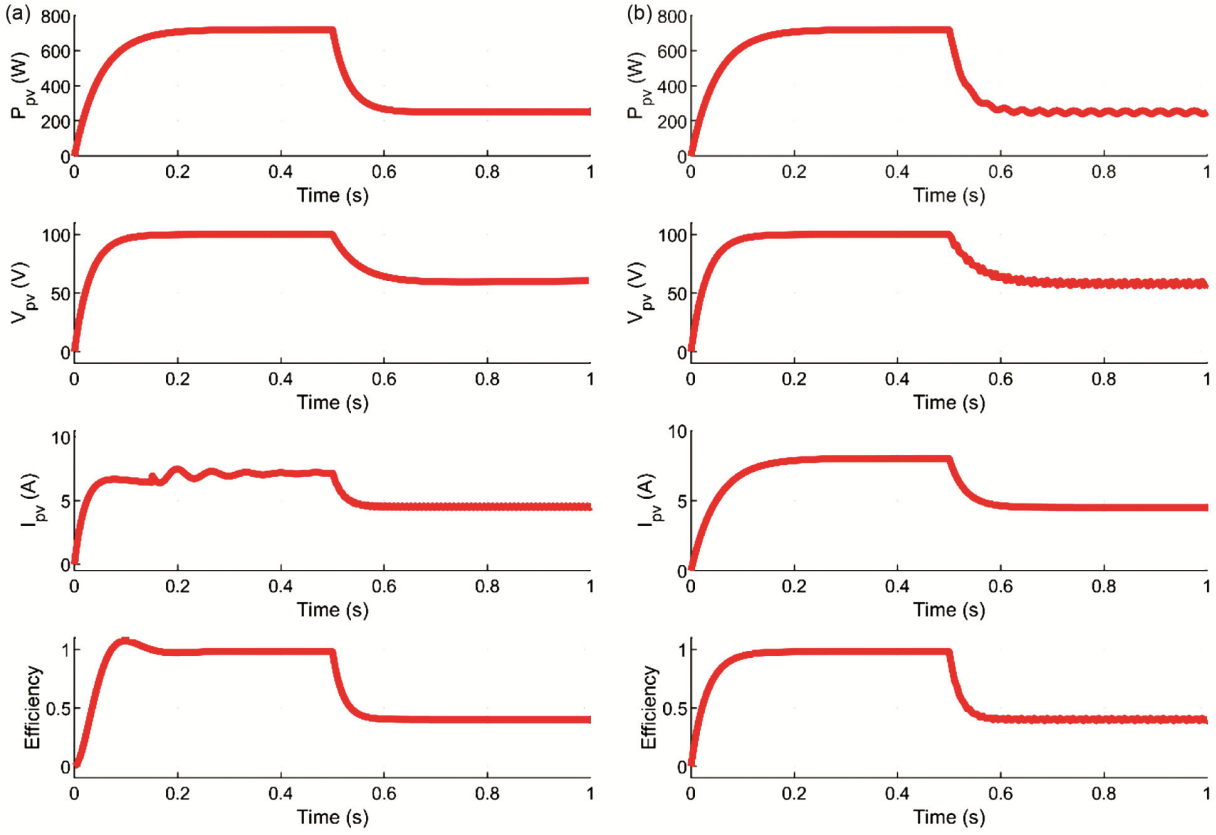

Fig. 22 — PV system in sudden change in irradiance from 1000 W/m² to 500 W/m² (a) Conventional P&O and (b) Proposed FLC-P&O-FLC controller.

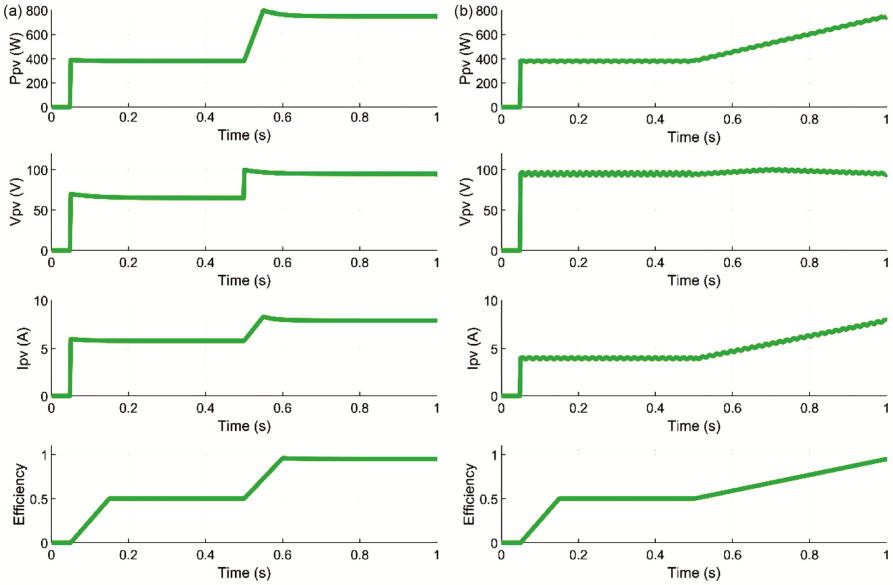

Fig. 23 — PV system in sudden change in irradiance from 500 W/m² to 1000 W/m² (a) Conventional P&O and (b) Proposed FLC-P&O-FLC controller.

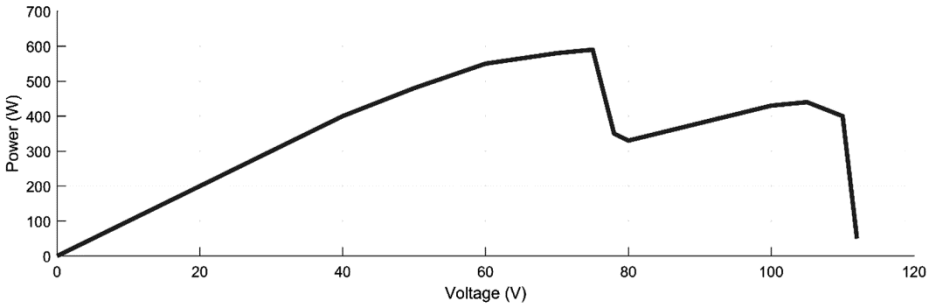

Fig. 24 — P-V curve output characteristics for the case of partial moderate shading.

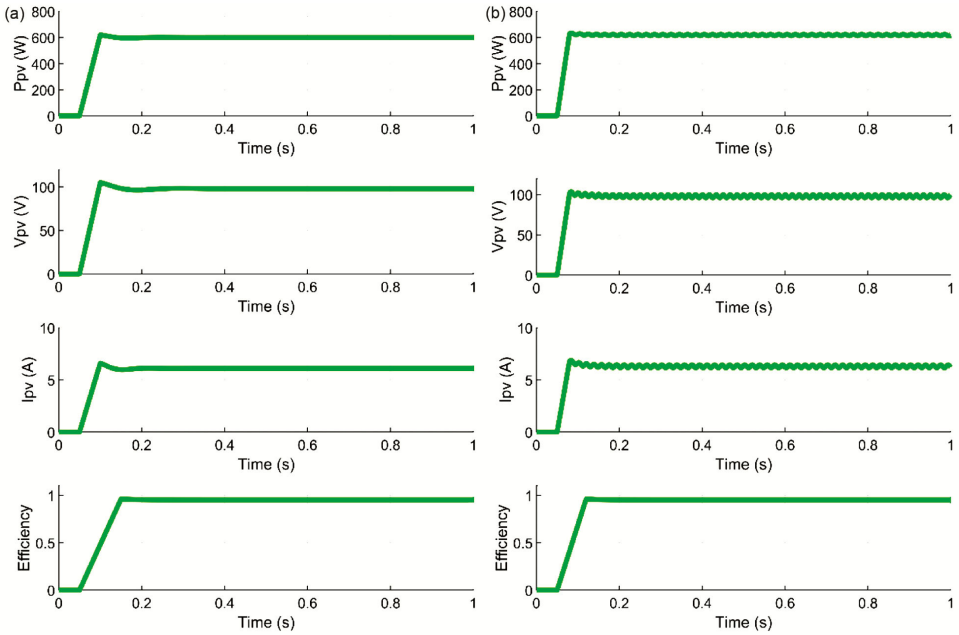

Fig. 25 — PV system in weak PSC (a) Conventional P&O and (b) Proposed FLC-P&O-FLC controller.

Table 5 — PV array incident irradiance at the GMPP and corresponding output power.

Case	PV Array Irradiation (W/m^2)	Power (W)
Strong PS	[1000;1000;250]	577.7
Moderate PS	[1000;1000;500]	577.9
Weak PS	[1000;1000;750]	657.1

Table 6 — Comparison of the suggested FLC-P&O-FLC controller's performance with that of conventional P&O under various conditions.

Parameter	Convention P&O	FLC-P&O-FLC
Tracking speed	Excellent	Outstanding
Steady-state error	Higher	Moderate
Obtaining actual MPP	No	Yes
Oscillation	Lower	Moderate

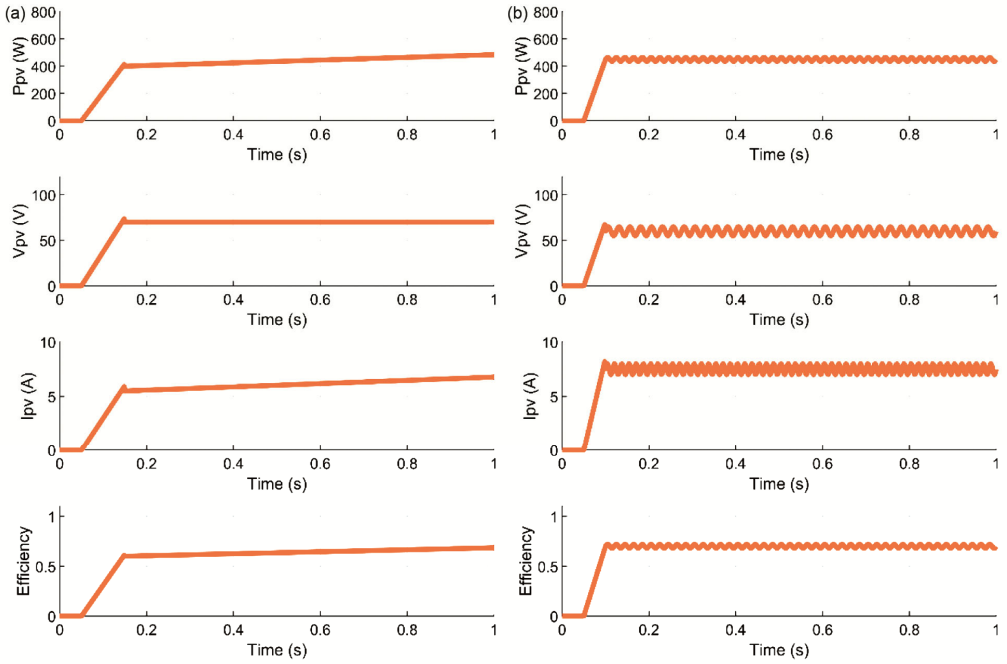

Fig. 26 — PV system in moderate PSC (a) Conventional P&O and (b) Proposed FLC-P&O-FLC controller.

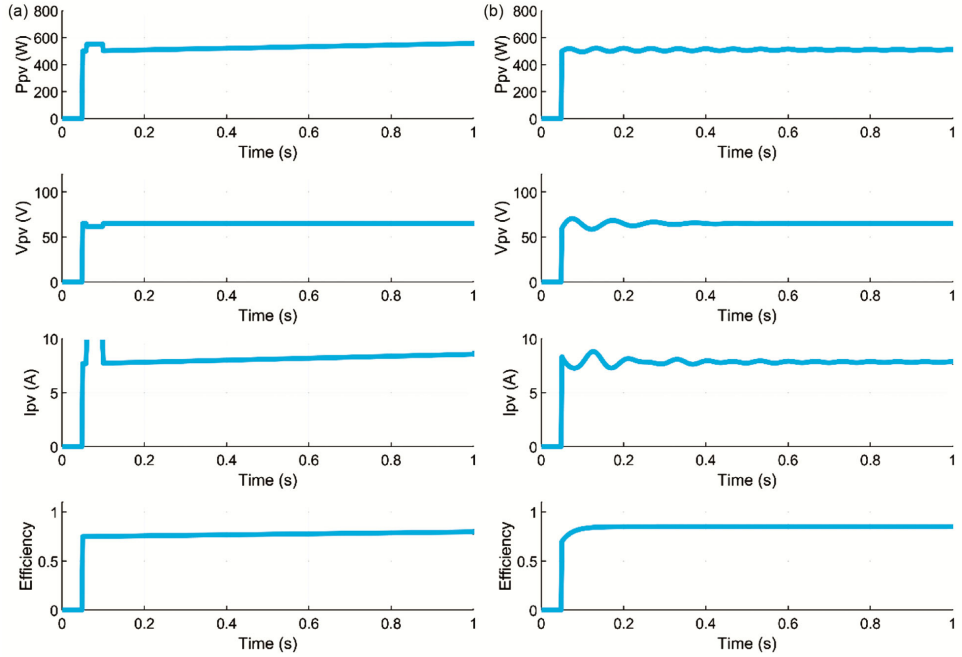

Fig. 27 — PV system in strong PSC (a) Conventional P&O and (b) Proposed FLC-P&O-FLC controller.

4 Conclusion

The proposed hybrid MPPT technique unites the benefits of the FLC and P&O algorithms in two stages of structure. In the first stage, an initial FLC is used for fast and intelligent estimation of the MPP to substitute traditional FLC slow convergence by leveraging the faster response features of the P&O. The second stage is then the dynamic tuning of the VSS of the P&O algorithm by a secondary FLC to compensate for the inherent trade-off of the conventional, fixed-step P&O methods between rapid tracking and steady-state oscillation. In particular, the VSS that accelerates the tracking process comes at the expense of large oscillations around the MPP, and one that limits the oscillations progresses rapidly but has a slow response to irradiance fluctuations. As a result of the adaptive real-time system condition-based VSS adjustment as implemented by the second FLC, the proposed hybrid MPPT overcomes this limitation and provides enhanced transient response as well as better steady-state precision. The proposed approach is validated through simulation results, which indicate it improves the tracking efficiency of P&O higher than conventional P&O in dynamic and nonuniform irradiance conditions.

Acknowledgements

The authors are thankful to the Department of Electrical Engineering, National Institute of Technology, Jamshedpur, Jharkhand, India.

References

1 Pujahari R M, Energy Materials (Elsevier), ISBN: 9780128237106, (2021), pp. 27–60.
2 Ramesh S, The Political Economy of Contemporary Human Civilisation, Vol II (Springer Nature Switzerland, Cham), ISBN: 9783031841859, (2025), pp. 183–218.
3 Tan K M, Babu T S, Ramachandaramurthy V K, et al., J Energy Storage, 39 (2021) 102591.
4 Hasan K, Yousuf S B, Tushar M S H K, et al., Energy Sci Eng, 10 (2022) 656–675.
5 Eltamaly A M, Photovoltaic Maximum Power Point Trackers: An Overview (Springer, Cham), (2021), pp. 117–200.
6 Elmetennani S, Laleg-Kirati T M, Djemai M, et al., J Process Control, 48 (2016) 14–24.
7 Al-Ezzi A S, Ansari M N M, Appl Syst Innov, 5 (2022) 67.
8 Remoaldo D, Jesus I, Algorithms, 14 (2021) 24.
9 Jabbar R I, Mekhilef S, Mubin M, et al., IEEE Access, 11 (2023) 76166–76176.
10 Alhusseini H, Niroomand M, Mirzaeian Dehkordi B, IEEE Access, 12 (2024) 84374–84386.
11 Chellakhi A, El Beid S, Abouelmahjoub Y, et al., Arab J Sci Eng, 49 (2024) 16045–16064.
12 Tang H H, Ahmad N S, Syst Sci Control Eng, 12 (2024) 2394429.
13 Macaulay J, Zhou Z, Energies, 11 (2018) 1340.
14 Wang Q G, Sun J, Zhang J X, et al., Control Eng Pract, 138 (2023) 105559.
15 Singhal A K, Beniwal N S, Beniwal R, et al., Energies, 15 (2022) 4251.
16 Nordin N A, Mohamed Ansari M N M, Nomanbhay S M, et al., Energies, 14 (2021) 7211.
17 Sun C, Zou Y, Qin C, et al., Adv Compos Hybrid Mater, 5 (2022) 2675–2699.
18 Raj A, Praveen R P, Ain Shams Eng J, 13 (2022) 101617.
19 Derbeli M, Napole C, Barambones O, et al., Energies, 14 (2021) 7806.
20 Ali M, Iqbal A, Khan M R, et al., Power Electronics Handbook (Elsevier), ISBN: 9780323992169, (2024), pp. 437–480.
21 Gonzalez-Castano C, Restrepo C, Kouro S, *et al*., IEEE Access, 9 (2021) 43121–43133.
22 Jacobo Tapia R, Shahbazi M, Microelectron Reliab, 135 (2022) 114583.
23 Başoğlu M E, Sol Energy, 241 (2022) 85–108.
24 Çakmak F, Aydoğmuş Z, Tür M R, Electr Power Components Syst, 52 (2024) 1528–1542.
25 Banik A, Shrivastava A, Potdar R M, et al., Mater Today Proc, 51 (2022) 756–763.
26 Uzun B, Uzun Ozsahin D, Duwa B, Fuzzy Logic and Fuzzy Based Multi Criteria Decision Analysis (Springer, Cham), ISBN:978-3-030-64765-0, (2021), pp. 47–56.
27 Siddique M A B, Zhao D, Rehman A U, et al., Sci Rep, 14 (2024) 9462.
28 Ali M N, Mahmoud K, Lehtonen M, et al., IEEE Access, 9 (2021) 26420–26430.
29 Eshete F A, Samajdar D P, Kumar A, Phys Scr, 99 (2024) 065212.